JOURNAL OF BIOMEDICAL OPTICS 3(2), 171–186 (APRIL 1998)

CORRECTION OF THE INTERNAL ABSORPTION EFFECT IN FLUORESCENCE EMISSION AND EXCITATION SPECTRA FROM ABSORBING AND HIGHLY SCATTERING MEDIA: THEORY AND EXPERIMENT

N. N. Zhadin and R. R. Alfano
New York State Center for Advanced Technology for Ultrafast Photonic Materials and Applications, Mediphotonics Laboratory, Institute for Ultrafast Spectroscopy and Lasers; The City College of The City University of New York, Department of Physics, New York, New York 10031

(Paper JBO-122 received Nov. 18, 1996; revised manuscript received Dec. 22, 1997; accepted for publication Jan. 10, 1997.)

ABSTRACT

Fluorescence spectra measured from biological samples, such as tissues or cell suspensions, are usually distorted due to the light absorption by intrinsic chromophores. These distortions are aggravated by strong scattering of light inside the samples. A new method is described for a fast correction of these spectral distortions, using only steady-state spectroscopic measurements. The method is based on the formulas derived from a simplified photon diffusion model, in the isotropic one-dimensional approximation applied to a semi-infinite, highly scattering, and moderately absorbing medium with a refractive-index-matched boundary. The formulas describe the spectral distortions of the fluorescence emission and excitation spectra, together with the diffuse reflectance spectrum, as the functions of one spectral characteristic of the medium, the darkness, which is the ratio of absorption coefficient and reduced scattering coefficient. The algorithm does not involve any iterative procedures, and offers a direct, simple, and fast method for real-time spectral correction. The true fluorescence emission or excitation spectrum is directly calculated from a pair of experimental spectra: the fluorescence emission or excitation spectrum and the diffuse reflectance spectrum, measured from the same position on a sample. The correction produces the profile of the true fluorescence spectrum, the same as the one measured from the corresponding sample with an infinitely low absorption and no scattering. The restoration of the spectral profiles of true fluorescence emission and excitation spectra was tested experimentally, using highly scattering phantoms with a fluorescent dye and a deliberately added nonfluorescent dye producing strong inner-filter distortions. [S1083-3668(98)00702-3]

Keywords fluorescence; internal absorption effect; inner-filter effect; re-absorption; multiple scattering; photon diffusion.

NOMENCLATURE OF DEFINITIONS

$\mu_a = \Sigma \sigma_{\mathrm{ap}} n_p$	linear absorption coefficient;
σ_{ap}	absorption cross section of pth chromophore;
n_p	number density of pth chromophore;
$\mu_s' = \Sigma (1 - g_q) \sigma_{\mathrm{sq}} n_q$	reduced scattering coefficient;
g_q	the mean cosine of scattering angle for qth scattering center;
σ_{sq}	scattering cross section of qth scattering center;
n_q	number density of qth scattering center;
$\mu_t = \mu_a + \mu_s'$	total attenuation coefficient;
$l = 1/\mu_s'$	photon transport mean free path (MFP) (scattering transport length);
$l_{\mathrm{dif}} = (3\mu_a\mu_s')^{-1/2}$	photon diffusion length;

Address all correspondence to Nick Zhadin, IUSL, Physics Dept., Rm. J-419, City College of New York, Convent Ave./138th Street, New York, NY 10031; Tel: (212)650-5531; Fax: (212)650-5530; E-mail: zhadin@scisun.sci.ccny.cuny.edu

$\delta = \mu_a / \mu_s'$	darkness;
λ_x	excitation wavelength;
λ_m	wavelength of fluorescence emission;
c	speed of light;
I	incident light intensity (photon flux);
α	incidence angle;
$R(\lambda) = I_r / I \cos \alpha$	diffuse reflectance;
I_r	total intensity of diffuse reflection;
$F(\lambda_m)$	intrinsic spectral intensity distribution function of fluorescence emission;
φ	fluorescence quantum yield (quantum efficiency);
μ_{fx}	linear absorption coefficient of fluorescent chromophores (fluorophores) at the excitation wavelength;
$T = kF\varphi\mu_{\mathrm{fx}}$	spectral intensity distribution function of the true fluorescence emission and excitation spectra (k is a normalization constant);
ρ	number density of photons (with all available wavelengths);
$\psi(\lambda) = \partial\rho / \partial\lambda$	spectral number density of photons (in the unit interval of wavelengths centered at the wavelength λ);
I_f	total intensity of fluorescence emission from the surface;
$i(\lambda_m, \lambda_x) = \partial I_f / \partial\lambda$	spectral intensity of fluorescence emission from the surface;
$J(\lambda_m, \lambda_x) = i(\lambda_m, \lambda_x) / I$	experimental fluorescence emission or excitation spectrum;
U	fluence rate;
z	linear coordinate (depth inside the medium);
indices:	
x	for values measured at the excitation wavelength;
m	for values measured at the emission wavelength.

1 INTRODUCTION

Fluorescence spectroscopy is extensively used in biology and is starting to be used in medicine. The native fluorescence from biological tissues[1] is becoming a viable approach to medical diagnostics. Fluorescence of extrinsic markers and contrasting agents, such as fluorescein, hematoporphyrin, etc., incorporated into biopolymers and membranes, added to living or excised biological tissues or to extracts from them, or patient-administered, is also an active field of investigation. Fluorescence spectra measured from biological samples are very often distorted due to the light absorption by intrinsic chromophores. This phenomenon of spectral distortion is known as inner-filter effect.[2] Additional dips or shoulders commonly appear in the observed emission and excitation spectra from biological tissues at the positions of the absorption bands of heme[3] or other molecules. The inner-filter effect is immensely strong in the spectra from biological media and other light-scattering samples because multiple scattering increases the path lengths of photons inside the sample. The resulting distortions of fluorescence spectra, such as false maxima, are sometimes misinterpreted. A demand exists for a convenient method to correct the inner-filter effect in the fluorescence spectra from biological samples.

The analysis of changes produced in the fluorescence spectra from biological tissues by the absorption of light by hemoglobin was performed by Liu et al.[3] They showed that the simplest approach of the straight propagation of light, which is applicable in the case of strong absorption and weak scattering, gives a satisfactory correction of the inner-filter distortions of fluorescence spectra near the long-wavelength end of the visible range. An experimental study of the combined effect of light scattering and absorption on the fluorescence spectra was reported by Ahmed et al.[4]

Over the past two decades, the theory of fluorescence from light-absorbing and scattering media became an active area of research.[5–33] The spatial distribution of the fluorescence emission from highly scattering samples was theoretically and experimentally studied by many authors.[6–11] The dependence between the fluorescence intensity and the concentration of fluorophores in highly scattering media was studied by Morton,[12] Allen,[13] Richards-Kortum et al.,[14] and by Sinaasappel and Sterenborg.[15] The effect of the detector-tissue separation on the fluorescence signal was investigated by Warren et al.[16] The dependence of the inner-filter effect on the geometry of the experiment for the fluorescence from tissues was analyzed by Keijzer et al.[17] An empirical relationship was found between total fluorescence intensity and the absorption coefficients of the medium at some selected wavelengths. Durkin et al.[18] obtained a corrective formula for the inner-filter effect, with the main accent on the overall fluorescence intensity. An effective removal of the inner-filter distortions from fluorescence emission spectra on the basis of the photon diffusion model and Monte Carlo simulations, using the diffuse reflectance spectrum as a

source of information about the sample absorption, was reported by Wu et al.[19,20] Patterson and Pogue,[21] using the photon diffusion model, showed that time-resolved and frequency-domain data can be used to eliminate the inner-filter distortions from fluorescence emission spectra. The temporal and spatial distributions of fluorescence intensities in scattering media, time- and frequency-domain parameters of the measured fluorescence, and their dependence on the scattering and absorption properties of the medium are extensively studied by the groups of Lakowicz and Sevick-Muraca,[22–27] Gratton,[28–31] Chance,[32] and by Gandjbakhche et al.[33] Nevertheless, up to the present time no simple algorithm has been offered for a real-time correction of the inner-filter effect in fluorescence spectra from biological and other turbid samples. No information was found about any attempts to make a correction of the inner-filter effect in the fluorescence excitation spectra from scattering media.

We report on a new direct analytical method to correct the inner-filter spectral distortions. This method can be used with standard, steady-state, spectroscopic equipment. The necessary properties of the sample medium are retrieved from the diffuse reflectance spectrum, as was done earlier by Morton,[12] Allen,[13] and Wu et al.[20]

A general analytical solution for the problem of fluorescence in highly scattering media in a three-dimensional anisotropic approach is impossible.[21] Our theoretical approach is based on a simplified model of the diffusion of photons in a strongly scattering and moderately absorbing medium. The photon diffusion model, in different approximations, was previously applied by many authors to the multiple scattering of light in biological tissues and model systems.[5,7,19–47] We use the isotropic, one-dimensional approximation permitting an exact solution that provides the spectral intensities of diffuse reflection and fluorescence in a closed form, without any computer simulations. Both the diffuse reflectance spectrum and the inner-filter distortions of the fluorescence spectra are determined by one wavelength-dependent function: the ratio $\delta(\lambda)$ of absorption coefficient and reduced scattering coefficient. This ratio, called darkness, can be directly calculated from the diffuse reflectance spectrum, and can also be used as an approximation to the absorption spectrum.

To test our correction method, we applied it to the emission and excitation spectra of fluorescent dyes in highly light-scattering solutions with different concentrations of an additional nonfluorescent absorber dye. The correction has produced the spectral profiles that are very close to those from the same fluorophores in the diluted nonscattering solutions.

Our correction formulas effectively eliminate the inner-filter distortions from the fluorescence emission spectra and satisfactorily correct the excitation spectra when the photon diffusion model is valid. Moreover, the distortions of excitation spectra due to their inherently nonlinear dependence on the absorption are also corrected by our formulas. The effect corrected by our method is broader than the inner-filter effect, and the name "*internal absorption effect*" is more appropriate here.

2 THEORETICAL MODEL

The linear scattering coefficients for most tissues in the visible and near UV spectral regions vary between 40 and 1000 cm^{-1} while the linear absorption coefficients are usually in the range 0.1–5 cm^{-1}.[48,49] In tissue slabs of several millimeter thickness, the incoming photons participate in numerous scattering events before they are absorbed or leave the slab. Therefore, the propagation of photons through the tissue is often described as a diffusion process.

We consider diffusion of photons in a uniform semi-infinite medium containing homogeneously distributed scattering centers, fluorescing chromophores (fluorophores), and nonfluorescing chromophores, as a model for a slab of tissue. We use the isotropic approximation in which photons, as an average, scatter isotropically after traveling the distance of the transport mean free path (MFP) $l = 1/\mu_s'$. Every isotropic act of scattering as an average consists of $(1-g)^{-1}$ actual small-angle scattering events, where g is the mean cosine of scattering angle. Considering the diffusion process within the frame of local and total balances of photons in the medium, we explicitly count the acts of photon absorption and assume the MFP l to be determined only by scattering events. Including the absorption component into the inverse MFP, as is often done when the transport of photons is considered, would lead in our case to a double accounting for the absorption. We assume that the medium is refractive-index matched on the boundary. We neglect all coherence effects, the secondary fluorescence emission after reabsorption of photons by fluorophores, and inelastic scattering events.

2.1 EXCITATION PHOTON NUMBER DENSITY AND DIFFUSE REFLECTANCE

In this section we find a distribution of the excitation photons in the medium and establish an analytical link between the diffuse reflectance spectrum and parameters of the medium.

An infinitely wide parallel beam of monochromatic excitation light, with the intensity I (the photon flux), is incident on the surface of the sample medium at an angle α from the normal. The z axis is directed into the medium, perpendicular to the boundary, with $z=0$ on the boundary.

The excitation light in the medium can be divided into two components: (1) isotropic (or nearly isotropic) component, i.e., diffusing photons, and (2) strongly anisotropic component, predominantly propagating along the initial incidence direction,

qualified as straight-propagating photons. The straight-propagating photons include: (a) nonscattered photons, and (b) photons that actually scattered a few number of times at small angles.

The anisotropic component of photons does not directly contribute into the reemission (diffuse reflection) from the surface, because these photons are moving inward. We assume that all reemission of photons is determined by the hits of diffusing photons into the boundary. One can easily show that the number of these hits in a unit of time, i.e., the total intensity of diffuse reflection from the surface, is equal to

$$I_r = \frac{c\rho_0}{4}, \tag{1}$$

where c is the speed of light, and ρ_0 is the number density of photons near the surface ($z=0$).

The balance of diffusing photons in a layer of infinitesimal thickness dz and unit area can be written as

$$\frac{\partial \rho}{\partial t}\, dz = \left(\frac{cl}{3}\, \frac{\partial^2 \rho}{\partial z^2} + \mu_s' I e^{-\mu_t z/\cos\alpha} - c\mu_a \rho \right) dz. \tag{2}$$

The three terms inside the brackets in Eq. (2) describe: (1) migration of diffusing photons, (2) conversion of the straight-propagating photons into diffusing photons in the layer (source density), and (3) absorption of the diffusing photons in the layer. The second, source-density term fades away at the depth z of a few MFPs, and is sometimes neglected. Nevertheless, in our steady-state case, this neglecting would significantly shift the equilibrium distribution of excitation photons near the surface of the medium, which is critical for both the diffuse reflectance and the fluorescence emission from the surface.

In the stationary case, $\partial\rho/\partial t = 0$, the resulting time-independent equation is

$$\frac{\partial^2 \rho}{\partial z^2} - \beta^2 \rho = -\frac{3I}{cl^2}\, e^{-\mu_t z/\cos\alpha}, \tag{3}$$

where $\beta = \sqrt{3\mu_a / l}$. Equation (3) has a solution satisfying the condition $\rho \to 0$ at $z \to \infty$

$$\rho = R\, \frac{4I\cos\alpha}{c}\, e^{-\beta z} + \frac{3I(e^{-(\mu_t/\cos\alpha)z} - e^{-\beta z})}{cl^2 \left(\beta^2 - \dfrac{\mu_t^2}{\cos^2\alpha} \right)}. \tag{4}$$

The second term on the right side of Eq. (4) is combined from a partial solution of Eq. (3) and a general solution of the corresponding homogeneous equation to eliminate the irregularity at $\mu_t/\cos\alpha = \beta$. This term goes to zero at $z=0$ and at $z \to \infty$. The coefficient at the first term is the photon number density ρ_0 at the surface. We expressed it using Eq. (1) and the definition of the diffuse reflectance. The diffuse reflectance R can be found from the total balance of excitation photons in the medium

$$I\cos\alpha = RI\cos\alpha + I\, \frac{\mu_a \cos\alpha}{\mu_t} + \int_0^\infty c\mu_a \rho\, dz. \tag{5}$$

The first term on the right side is the total diffuse reflection intensity, the second term describes the absorbed straight-propagating photons, and the third term represents absorption of the diffusing photons in the medium. This yields the reflectance to be

$$R(\lambda) = \frac{1}{\left(1 + \dfrac{4}{\sqrt{3}}\, \sqrt{\delta} \right)(\delta + \sqrt{3\delta}\cos\alpha + 1)}, \tag{6}$$

where

$$\delta(\lambda) \equiv \mu_a(\lambda) l(\lambda) = \frac{\mu_a(\lambda)}{\mu_s'(\lambda)} \tag{7}$$

is the product of the absorption coefficient and photon MFP or the ratio of absorption coefficient and reduced scattering coefficient, defined as *darkness*. High values of δ result in a low return of photons by the scattering and absorbing medium, which explains the name *darkness*.

The reflectance $R(\lambda)$ is a monotonic function of darkness, and Eq. (6) can be resolved for the darkness $\delta(\lambda)$ as a function of reflectance $R(\lambda)$

$$\delta(\lambda) = \left(P^{1/3} - \frac{A}{P^{1/3}} - B \right)^2,$$

$$P(\lambda) = \frac{\sqrt{3}}{8} \left[\left(\frac{1}{R} - 1 \right) - E + \sqrt{\left(\frac{1}{R} - 1 \right)^2 - 2E\left(\frac{1}{R} - 1 \right) - G} \right],$$

$$A = \tfrac{1}{48}\,(15 + 4\cos\alpha - 16\cos^2\alpha),$$

$$B = \frac{\sqrt{3}}{12}\,(4\cos\alpha + 1), \tag{8}$$

$$E = \tfrac{1}{72}\,(4\cos\alpha + 1)(16\cos^2\alpha - 10\cos\alpha - 23),$$

$$G = \frac{1}{1296}\,(3\cos\alpha + 4)^2 (48\cos^2\alpha - 24\cos\alpha - 61).$$

Equations (8) offer a practical way to find the darkness spectrum $\delta(\lambda)$ from the experimentally measured diffuse reflectance spectrum $R(\lambda)$.

2.2 FLUORESCENCE FROM HIGHLY SCATTERING MEDIUM

All parameters with the subscript x correspond to the excitation wavelength λ_x, and the parameters with the subscript m correspond to the emission wavelength λ_m.

The spectral intensity of surface fluorescence emission at the wavelength λ_m, when the excitation light has the wavelength λ_x, is defined as a function of these wavelengths: $i_f(\lambda_m,\lambda_x)\equiv(dI_f/d\lambda)_{\lambda_m}$, where I_f is the total intensity of the fluorescence emission from the surface. The spectral fluorescence intensity $i_f(\lambda_x,\lambda_m)$ divided by the intensity of the excitation light $I(\lambda_x)$ represents the experimentally measured fluorescence emission or excitation spectrum

$$J(\lambda_m,\lambda_x)=\frac{i_f(\lambda_m,\lambda_x)}{I(\lambda_x)}. \tag{9}$$

When the emission wavelength λ_m is variable, with the fixed excitation wavelength λ_x, this function represents the emission spectrum. When the excitation wavelength λ_x is variable, and the emission wavelength λ_m is fixed, the function $J(\lambda_m,\lambda_x)$ represents the excitation spectrum.

The profile of the *true* fluorescence emission or excitation spectrum is represented by the product of the intrinsic emission intensity distribution function $F(\lambda_m)$, the fluorescence quantum yield $\varphi(\lambda_x)$, and the absorption coefficient of fluorophores $\mu_{\rm fx}(\lambda_x)$ at the excitation wavelength

$$T(\lambda_m,\lambda_x)=kF(\lambda_m)\varphi(\lambda_x)\mu_{\rm fx}(\lambda_x), \tag{10}$$

where k is a constant. The wavelength profile of the true fluorescence emission spectrum $T_{\rm EM}(\lambda_m)$ is determined by the function $F(\lambda_m)$. The profile of the true excitation spectrum $T_{\rm EX}(\lambda_x)$ is determined by the product $\varphi(\lambda_x)\mu_{\rm fx}(\lambda_x)$. In our mathematical formalism we assume for brevity that only one type of fluorophores is emitting fluorescence light, but our derivation can be easily generalized for several types of fluorophores.

The experimentally measured fluorescence emission and excitation spectra from a *very weakly* absorbing and nonscattering sample, with only one fluorophore and no other chromophores, are close in their shapes to the true spectra. In this case, the excitation spectrum usually provides an estimate for the shape of the fluorophore absorption spectrum $\mu_{\rm fx}$ because fluorescence quantum yield $\varphi(\lambda_x)$ for most of organic molecules usually shows only minor if any dependence on the excitation wavelength (see, for example, Ref. 50). Practically, the excitation spectra, even from moderately absorbing samples, are often difficult to interpret because of their nonlinear dependence on $\mu_{\rm fx}$ and because of a strong distorting effect of other absorbers.

Fluorescence emission arising from the surface of a highly scattering medium is due to the hits of the diffusing fluorescence photons upon the boundary from inside. Similar to Eq. (1), the total intensity of this fluorescence emission is determined by the number density of fluorescence photons near the surface: $I_f=c\rho_{f0}/4$. The number density of photons having their wavelengths within the band $d\lambda$ at the emission wavelength λ_m is $d\rho_{\rm fm}=(\partial\rho_f/\partial\lambda)_{\lambda_m}d\lambda \equiv\psi_m d\lambda$, where ψ_m is the spectral number density of fluorescence photons at the wavelength λ_m. The stationary balance of fluorescence photons in the unit-square layer of an infinitesimal thickness dz is

$$\begin{aligned}\frac{\partial\rho_f}{\partial t}\,dz=\int_0^\infty\Big[&F(\lambda_m)\varphi\rho_x c\mu_{\rm fx}dz\\&+IF(\lambda_m)\varphi\mu_{\rm fx}e^{-(\mu_{tx}/\cos\alpha)z}dz+\frac{cl_m}{3}\frac{\partial^2\psi_m}{\partial z^2}\,dz\\&-\psi_m c\mu_{\rm am}dz\Big]d\lambda_m=0.\end{aligned} \tag{11}$$

The four terms in the square brackets describe: (1) fluorescence excitation by the diffusing photons, (2) fluorescence excitation by the straight-propagating photons, (3) diffusion migration of the fluorescence photons, and (4) their absorption, respectively. The number density of excitation photons ρ_x can be substituted from Eq. (4), and Eq. (11) yields a time-independent differential equation in which the spectral number density of fluorescence photons ψ_m is the unknown function of the coordinate z

$$\begin{aligned}\frac{\partial^2\psi_m}{\partial z^2}-\beta_m^2\psi_m=&-\frac{3IF\varphi\mu_{\rm fx}}{cl_m}\,e^{-(\mu_{\rm tx}/\cos\alpha)z}\\&-\frac{12IF\varphi\mu_{\rm fx}\cos\alpha}{cl_m}\,R_x e^{-\beta_x z}\\&-\frac{9IF\varphi\mu_{\rm fx}}{cl_x^2 l_m\left(\beta_x^2-\dfrac{\mu_{\rm tx}^2}{\cos^2\alpha}\right)}\\&\times(e^{-(\mu_{\rm tx}/\cos\alpha)z}-e^{-\beta_x z}).\end{aligned} \tag{12}$$

The solution of this equation satisfying the condition $\psi_m\to 0$ at $z\to\infty$ is

$$\begin{aligned}\psi_m=\psi_{m0}e^{-\beta_m z}+&\frac{3IF\varphi\mu_{\rm fx}}{cl_m}\left[1+\frac{3}{l_x^2\left(\beta_x^2-\dfrac{\mu_{\rm tx}^2}{\cos^2\alpha}\right)}\right]\\&\times\frac{e^{-(\mu_{\rm tx}/\cos\alpha)z}-e^{-\beta_m z}}{\beta_m^2-\dfrac{\mu_{\rm tx}^2}{\cos^2\alpha}}+\frac{3IF\varphi\mu_{\rm fx}}{cl_m}\\&\times\left[4R_x\cos\alpha-\frac{3}{l_x^2\left(\beta_x^2-\dfrac{\mu_{\rm tx}^2}{\cos^2\alpha}\right)}\right]\\&\times\frac{e^{-\beta_x z}-e^{-\beta_m z}}{\beta_m^2-\beta_x^2}.\end{aligned} \tag{13}$$

The spectral number density of fluorescence photons on the boundary $\psi_{m0}=\psi_m(0)$, determines the spectral intensity of the fluorescence collected from the surface at all angles within the solid angle 2π: $i_f=c\psi_{m0}/4$. This spectral intensity can be found from the total stationary balance of fluorescence photons in the medium, by integrating all generated, absorbed, and emitted photons at all depths and all wavelengths. The result is

$$i_f(\lambda_m,\lambda_x)=\frac{IF\varphi\mu_{\mathrm{fx}}l_x\cos\alpha}{1+\frac{4}{\sqrt{3}}\sqrt{\delta_m}}\left[\frac{4}{\sqrt{3}}\frac{R_x}{\sqrt{\delta_x}+\frac{l_x}{l_m}\sqrt{\delta_m}}+\frac{\sqrt{3}\cos\alpha}{(1+\delta_x+\sqrt{3\delta_x}\cos\alpha)\left(1+\delta_x+\frac{l_x}{l_m}\sqrt{3\delta_m}\cos\alpha\right)\left(\sqrt{\delta_x}+\frac{l_x}{l_m}\sqrt{\delta_m}\right)}+\frac{1}{1+\delta_x+\frac{l_x}{l_m}\sqrt{3\delta_m}\cos\alpha}\right]. \tag{14}$$

There are no singularities in Eq. (14), because $\delta_x \geqslant \mu_{\mathrm{fx}}l_x$.

In Eq. (14) the diffuse reflectance R_x is directly measured, δ_x and δ_m can be calculated using Eq. (8) from the measured diffuse reflectances R_x and R_m. Photon MFPs l_x and l_m are much more difficult to measure, but their ratio, which is used in Eq. (14), can be evaluated assuming $\sigma_s\propto 1/\lambda^p$ wavelength dependence of scattering cross section and a weak wavelength dependence of the mean cosine g of the scattering angle. These assumptions are correct for different scattering media,[5] including human tissues.[48,49] In this case, $l\propto\lambda^p$, and

$$\frac{l_x}{l_m}=\left(\frac{\lambda_x}{\lambda_m}\right)^p. \tag{15}$$

The power p in the wavelength dependence of scattering cross section and photon MFP depends on the size of particles or the medium inhomogeneities that determine scattering.[5] It varies from $p=4$ in the Rayleigh limit, when the scattering particles are much smaller than the wavelength of light, to $p=0$ for scattering on very large particles. In practice, the value of power p can be either predetermined when the scattering properties of the sample medium are known, or found experimentally from an application of the correction procedure to a standard sample with similar scattering properties and known shape of the true fluorescence spectrum.

Substituting i_f from Eq. (14) into Eq. (9) and using Eq. (15), we obtain a formula for the experimental fluorescence spectrum as a function of the intrinsic parameters of fluorophores and practically measurable parameters of the medium

$$J(\lambda_m,\lambda_x)=\frac{F\varphi\mu_{\mathrm{fx}}l_x\cos\alpha}{1+\frac{4}{\sqrt{3}}\sqrt{\delta_m}}\left\{\frac{4}{\sqrt{3}}\frac{R_x}{\sqrt{\delta_x}+\left(\frac{\lambda_x}{\lambda_m}\right)^p\sqrt{\delta_m}}+\frac{\sqrt{3}\cos\alpha}{[1+\delta_x+\sqrt{3\delta_x}\cos\alpha]\left[1+\delta_x+\left(\frac{\lambda_x}{\lambda_m}\right)^p\sqrt{3\delta_m}\cos\alpha\right]\left[\sqrt{\delta_x}+\left(\frac{\lambda_x}{\lambda_m}\right)^p\sqrt{\delta_m}\right]}+\frac{1}{1+\delta_x+\left(\frac{\lambda_x}{\lambda_m}\right)^p\sqrt{3\delta_m}\cos\alpha}\right\}. \tag{16}$$

2.3 CORRECTION OF THE FLUORESCENCE EMISSION SPECTRA

The profile of the true fluorescence emission spectrum can be obtained now from Eqs. (10) and (16)

$$T_{\mathrm{EM}}(\lambda_m,\lambda_x)=\frac{J(\lambda_m,\lambda_x)}{NY(\lambda_m,\lambda_x)}, \tag{17}$$

where the coefficient

$$N(\lambda_x)=\frac{l_x\cos\alpha}{k} \tag{18}$$

does not depend on the variable emission wavelength and can be considered as a normalization constant; and $Y(\lambda_m,\lambda_x)$ is the *emission correction factor*

$$Y(\lambda_m,\lambda_x)=\frac{1}{1+\frac{4}{\sqrt{3}}\sqrt{\delta_m}}\left\{\frac{4}{\sqrt{3}}\frac{R_x}{\sqrt{\delta_x}+\left(\frac{\lambda_x}{\lambda_m}\right)^p\sqrt{\delta_m}}+\frac{\sqrt{3}\cos\alpha}{[1+\delta_x+\sqrt{3\delta_x}\cos\alpha]\left[1+\delta_x+\left(\frac{\lambda_x}{\lambda_m}\right)^p\sqrt{3\delta_m}\cos\alpha\right]\left[\sqrt{\delta_x}+\left(\frac{\lambda_x}{\lambda_m}\right)^p\sqrt{\delta_m}\right]}+\frac{1}{1+\delta_x+\left(\frac{\lambda_x}{\lambda_m}\right)^p\sqrt{3\delta_m}\cos\alpha}\right\}. \tag{19}$$

2.4 EMISSION SPECTRUM CORRECTION ALGORITHM

We offer a procedure to obtain the profile of the true fluorescence emission spectrum $T_{\mathrm{EM}}(\lambda_m,\lambda_x)$: (1) measure the fluorescence emission spectrum $J(\lambda_m,\lambda_x)$ for the fixed excitation wavelength λ_x and variable emission wavelength λ_m; (2) measure the diffuse reflectance spectrum $R(\lambda)$ from the same position on the sample, in the spectral range including both the excitation wavelength λ_x and the whole range of the emission spectrum; (3) calculate the spectrum of darkness $\delta(\lambda)$ using Eq. (8); (4) substitute $\delta(\lambda)$ into Eq. (19) and calculate the correction factor $Y(\lambda_m,\lambda_x)$; and (5) use Eq. (17) with an appropriate normalization constant N to obtain the true spectrum of fluorescence emission $T_{\mathrm{EM}}(\lambda_m,\lambda_x)$.

2.5 CORRECTION OF THE FLUORESCENCE EXCITATION SPECTRA

To be practically applicable for correction of fluorescence excitation spectra, Eqs. (14) and (16) must be rearranged to get a stand-alone constant l_m instead of a stand-alone variable l_x. Multiplying the whole of Eq. (14) and all of its denominators in the square brackets by l_m/l_x, using Eqs. (15) and (10), we obtain the profile of the true excitation spectrum $T_{\mathrm{EX}}(\lambda_x,\lambda_m)$

$$T_{\mathrm{EX}}(\lambda_m,\lambda_x)=\frac{i_f(\lambda_m,\lambda_x)}{MW(\lambda_m,\lambda_x)}, \tag{20}$$

where the coefficient

$$M(\lambda_m)=\frac{l_m\cos\alpha}{k\left(1+\frac{4}{\sqrt{3}}\sqrt{\delta_m}\right)} \tag{21}$$

does not depend on the variable excitation wavelength and in practice is an arbitrary constant. The excitation-wavelength-dependent quotient $W(\lambda_m,\lambda_x)$ is the *correction factor for excitation spectrum*

$$W(\lambda_m,\lambda_x)=\frac{4}{\sqrt{3}}\frac{R_x}{\sqrt{\delta_m}+\left(\frac{\lambda_m}{\lambda_x}\right)^p\sqrt{\delta_x}}+\frac{\sqrt{3}\cos\alpha}{[1+\delta_x+\sqrt{3\delta_x}\cos\alpha]\left[(1+\delta_x)\left(\frac{\lambda_m}{\lambda_x}\right)^p+\sqrt{3\delta_m}\cos\alpha\right]\left[\sqrt{\delta_x}+\left(\frac{\lambda_x}{\lambda_m}\right)^p\sqrt{\delta_m}\right]}+\frac{1}{(1+\delta_x)\left(\frac{\lambda_m}{\lambda_x}\right)^p+\sqrt{3\delta_m}\cos\alpha}. \tag{22}$$

2.6 EXCITATION SPECTRUM CORRECTION ALGORITHM

To obtain the profile of the true fluorescence excitation spectrum $T_{EX}(\lambda_x,\lambda_m)$ we offer the procedure: (1) measure the fluorescence excitation spectrum $J(\lambda_x,\lambda_m)$ for the fixed emission wavelength λ_m and variable excitation wavelength λ_x; (2) measure the diffuse reflectance spectrum $R(\lambda)$ from the same position on the sample, in the spectral range including both the emission wavelength λ_m and the whole range of the excitation spectrum; (3) calculate the spectrum of darkness $\delta(\lambda)$ using Eq. (8); (4) substitute $\delta(\lambda)$ into Eq. (22) and calculate the correction factor $W(\lambda_x,\lambda_m)$; and (5) calculate the true fluorescence excitation spectrum $T_{EX}(\lambda_x,\lambda_m)$ from Eq. (20) using an appropriate normalization constant M.

3 ANALYSIS OF THEORETICAL RESULTS

3.1 THE EFFECT OF THE MEDIUM ABSORPTION AND SCATTERING PROPERTIES ON SPECTRAL DISTORTIONS

The internal absorption effect strongly depends on the depth of penetration of the excitation light into the sample. Equation (4) describes the depth dependence of the excitation photon number density $\rho = \rho_x(z)$ within the semi-infinite slab of highly scattering material illuminated by a wide beam (plane wave) of light. The depth profile of the total intensity (fluence rate) $U(z)$ of the excitation light inside the medium can be found as the sum of the flux of straight-propagating photons (first term) and the diffuse intensity produced by randomly moving photons (second term)

$$U = I \cos\alpha e^{-(\mu_t/\cos\alpha)z} + c\rho. \qquad (23)$$

The graphs of fluence rate $U(z)$, for three values of the incidence angle α (0°, 30°, and 60°) and five different values of darkness δ (0, 0.0001, 0.001, 0.01, and 0.1) are shown in Figure 1 in dimensionless form: the depth is measured in the units of the photon MFP. The curves for a practically unrealistic extreme case $\delta = 0$, when the whole of the semi-infinite medium is almost uniformly filled with photons that can escape only through the surface, are shown for comparison only.

The salient features of Figure 1 are the following: (1) The excitation intensity in the scattering medium is several times higher than the incident intensity, due to retention of photons near the surface of the medium as a result of multiple scattering. (2) The maximum of the excitation intensity in the scattering medium is located not at the surface, but *under* the surface, at a depth of 0.5–3 MFPs depending on the darkness δ and the incidence angle α. These results are in agreement with the theoretical and experimental data obtained by Profio and Doiron,[7] who used the transport equation; by Flock et al.,[40] who used diffusion theory, and Monte Carlo simulations; and by Welch's group[51] that used diffusion theory and discrete ordinate approximation to the transport theory.

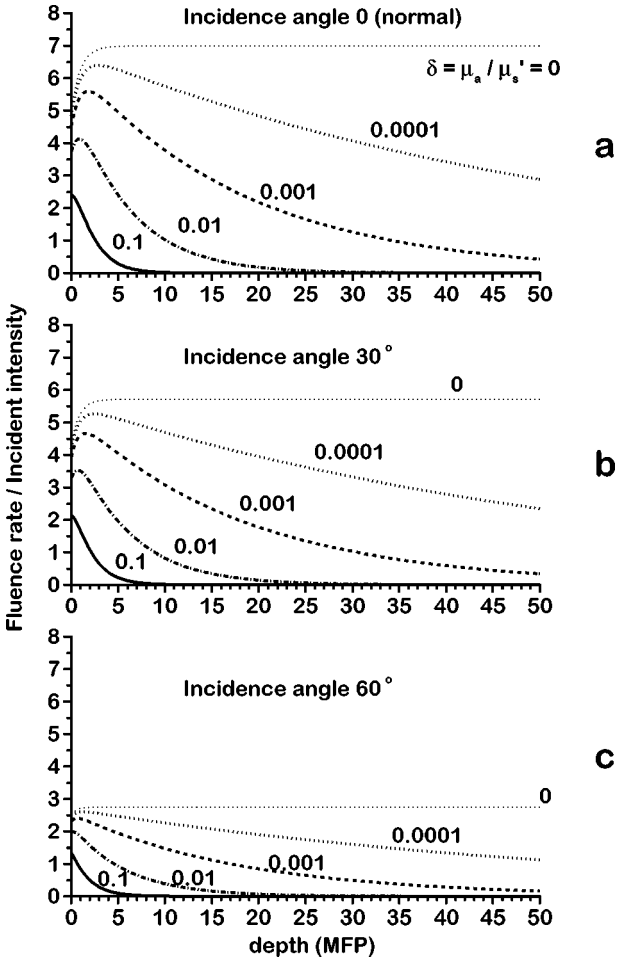

Fig. 1 The fluence rate of the excitation light inside the semi-infinite highly scattering medium as a function of the depth. The fluence rate is divided by the intensity of the incident light. The depth is measured in the units of the MFP of photons. (a) normal incidence, (b) incidence angle 30°, (c) incidence angle 60°.

The resulting distributions of the fluorescence photons in the medium, calculated from the expanded Eq. (13), are shown in Figure 2. All the depth profiles $\psi_m(z)$ are normalized at the boundary ($z = 0$). These distributions are similar to those of the excitation photons, but the maxima are shifted deeper into the medium. A decrease in the absorption of the fluorescence photons (lower values of δ_m) brings the spread of the photon distribution into the deeper layers of the medium.

Figure 3 shows the dependence of the normalized correction factors for fluorescence emission and excitation spectra on the darkness values δ_m and δ_x. Lower values of correction factors correspond to stronger inner-filter distortions of the fluorescence spectra. The weaker the absorption of the excitation light, the more significant the distortion of the fluorescence emission spectrum due to a deeper penetration of the excitation light into the medium

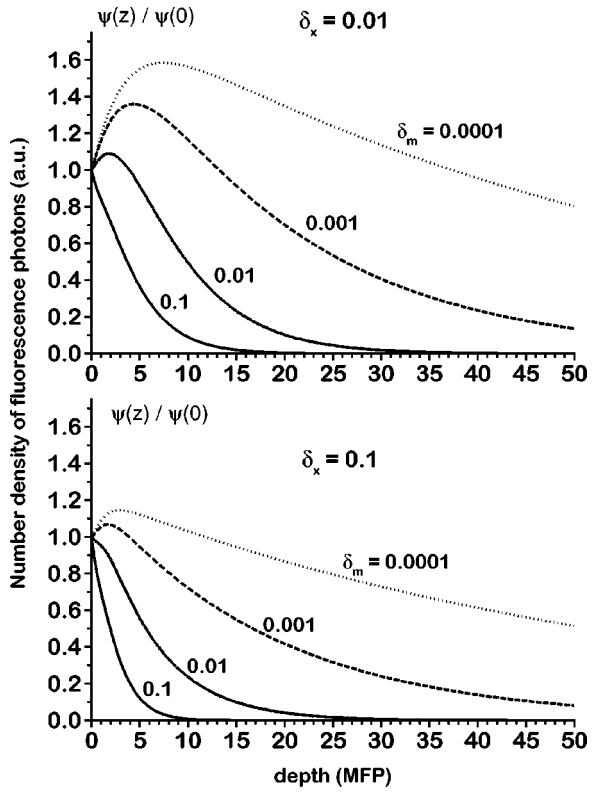

Fig. 2 The normalized number density of the fluorescence emission photons inside the semi-infinite highly scattering medium as a function of the depth. The depth is measured in the units of the MFP of photons.

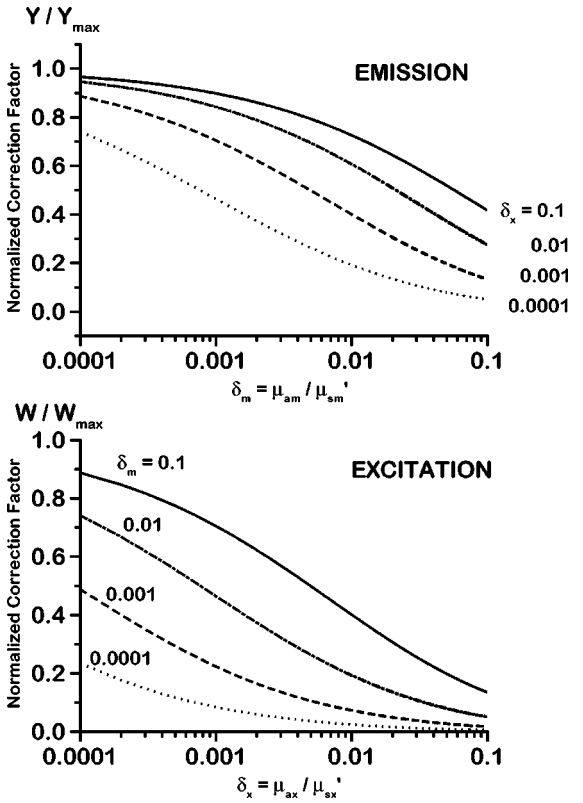

Fig. 3 Graphical presentation of Eqs. (19) and (22). The normalized correction factors for fluorescence emission spectra (upper graph) are shown as functions of the darkness δ_m at the emission wavelength, for three different values of the darkness δ_x at the excitation wavelength. The normalized correction factors for fluorescence excitation spectra (lower graph) are presented as functions of the darkness δ_x at the excitation wavelength, for three different values of the darkness δ_m at the emission wavelength. The curves for the incidence angles 0°, 30°, and 60° practically coincide.

(compare with Figure 1). When the absorption of the excitation light is strong enough ($\delta_x = 0.1$), the fluorescence spectrum appears almost nondistorted even at moderate absorption ($\delta_m < 0.01$) in the wavelength range of fluorescence.

Figure 3 also shows that the excitation spectra depend more strongly on the darkness δ than the emission spectra. The excitation spectrum correction factor sharply falls with the increase in the darkness δ_x at the excitation wavelengths. As a result, the excitation spectra appear distorted at low values of the darkness δ. This distortion grows only weakly with the further increase in the darkness. This is confirmed by our experimental data.

It is important to note that the distortion of the excitation spectrum is stronger when the absorption of the fluorescence emission is lower. The explanation of this result is viewed as the following: when this absorption is weaker, the fluorescence light can reach the surface from the deeper layers of the medium (see Figure 2). The excitation light coming to these deep layers is significantly distorted by the internal absorption, which results in stronger distortion of the excitation spectrum.

4 EXPERIMENTAL TESTING

4.1 EXPERIMENTAL PROCEDURES

We tested our correction method on the phantoms with dyes in scattering solutions commonly used to model the biological media. The sample size, and its absorption and scattering properties, were determined from the following considerations:

(a) The diffusion model is principally valid only in highly scattering media when the reduced scattering coefficient μ_s' is much greater than the absorption coefficient μ_a, i.e., $\delta \ll 1$.

(b) In our simplified approach, we considered the sample as a semi-infinite medium, which practically means that all the sample dimensions and the width of the light beam must be much greater than both the MFP of photons and the photon diffusion length $l_{\mathrm{dif}} = 1/\beta$.

A regular quartz 10 mm×10 mm cuvette cell was used in all measurements and the sample volume was 2 ml. The main limiting factor was the width of the excitation beam. The beam had a roughly rectangular cross section of 2 mm×8 mm. We used three kinds of samples. For the first group, the MFP was 0.13 mm, and the diffusion length at 550 nm

was 0.3–0.5 mm, which are both within the necessary range, but the MFP is shorter than in the commonly used biological samples. For the second group of samples, the MFP was 0.25 mm, and the diffusion length was 0.4–0.6 mm. These values are still within the validity range of the model, and close to the parameters of many biological media. The third group of samples had the parameters close to those of many other biological samples, but the MFP of 1 mm and the diffusion lengths of 0.9–1.3 mm were comparable with the beam width.

The spectral measurements were performed on the Perkin-Elmer LS-50 fluorescence spectrometer with the two single monochromators (Perkin-Elmer Corp., Norwalk, CT). The sample was illuminated by the light from the excitation monochromator at the angle $30° \pm 6°$ from the normal. The light of fluorescence or diffuse reflection was collected from the illuminated surface of the sample within the solid angle of about 0.25 sr centered at the angle 60° from the normal. For the measurements of emission spectra, a narrow-band filter (from Andover Corp., Salem, NH, or from Oriel Instruments, Stanford, CT; full width at half maximum (FWHM)=10 nm) for a corresponding excitation wavelength was inserted into the excitation beam to eliminate the stray light of the excitation monochromator. A long-pass glass filter (3-71; Corning Inc., Corning, NY) was inserted before the emission monochromator to eliminate the excitation light scattered by the sample. No correction was done for the emission channel spectral sensitivity. For the excitation spectra measurements, a corresponding narrow-band filter was placed at the input of the emission monochromator, and a short-pass filter (600 nm cutoff; Oriel Instruments, Stanford, CT) was placed at the output of the excitation monochromator to decrease the stray light level. The excitation spectra were divided by the transmission spectrum of the short-pass filter.

The diffuse reflectance spectra were measured directly before or after the fluorescence measurements, without moving the sample, in the synchroscan mode of the spectrometer (the excitation and emission monochromators synchronously scanning the same wavelengths). The 1:25 and 1:50 light-attenuating mesh filters were inserted into the excitation and emission beams, respectively, to allow the diffuse reflectance measurements using the same sensitivity and the same spectral resolution as in the fluorescence measurements. As the reference samples for the reflectance measurements, we used a certified Spectralon™ 99% Reflection Standard (Labsphere, North Sutton, NH) which has a Lambertian angular distribution of reflection, or the quartz cell with the maximal used concentration of scatterer (5% Intralipid). The spectral profile of the synchroscan spectrum from the Reflection Standard was corrected to 100% reflection using the manufacturer-supplied calibration data. To be used as a reference spectrum, the synchroscan spectrum from the 5% Intralipid solution was corrected to 100% reflectance using the reflectance data independently measured with the angular integration. The data produced with both reflection references were practically the same except for minor narrow peaks coming from the stray light. The stray light of the excitation monochromator, which cannot be reduced by the external devices in the synchroscan mode, pronounces itself in the spectra in a different way, depending on minor differences in the reflection angular distribution. The 5% Intralipid reference has the same angular distribution of the scattered light as the fluorescent samples, which results in a significant compensation of the stray light influence on our corrected spectra.

The spectral widths of both the excitation and emission monochromators were 4 nm in all fluorescence measurements. In the diffuse reflectance measurements, the spectral width of each monochromator was set to 8 nm that, due to the addition of the dispersions, resulted in the total 4 nm spectral width, the same as in the fluorescence. This value of the spectral width is small enough not to cause any significant distortion of the spectra.

To test the correction algorithm for fluorescence emission spectra, the following measurements were performed on several dye phantoms. The fluorescence and diffuse reflectance spectra were first recorded from a highly scattering solution of the Intralipid containing a fluorescent proflavine (PF) dye complex with DNA. Then a small amount (20 μl in a first portion, and 30 μl in a second portion) of a concentrated aqueous solution of nonfluorescent Basic Fuchsine (BF) dye was added to the sample, and the spectral measurements were repeated. The resulting molar concentrations of BF were 0.09 and 0.22 mM, respectively. The same measurements were done for similar samples without the fluorescing PF-DNA complex to obtain the background spectra. These background spectra were subtracted from the spectra of the samples with fluorescing complex to minimize contributions from stray light and fluorescence of impurities. The background intensities did not exceed 1% of the fluorescence intensity from the samples with the PF-DNA complex. This background subtraction is an optional procedure of measurement and has no relevance to the correction method.

Data processing was performed using LabCalc software (Galactic Industries Corp., Salem, NH) with the self-made extensions written in Array Basic™ programming language.

4.2 MATERIALS

Proflavine (3,6-diamino acridine) hemisulfate dihydrate (Fluka, >99% purity) was used as the fluorescing dye in the experiments for the emission spectra correction. In the experiments on the excitation spectra correction, we used the Kiton Red 620 dye (Sulforhodamine 620, laser grade; Exciton,

Inc., Dayton, OH) as a fluorophore. A nonfluorescent triphenyl methane dye Basic Fuchsine (Pararosaniline chloride, Aldrich, >96% purity) was used as the absorber.

To separate in space the fluorescent dye from the absorber dye and scattering particles, to prevent formation of nonfluorescing complexes, and to minimize resonant energy transfer, we used a complex of the proflavine fluorescent dye with DNA. It is known that the positively charged 3,6-diamino acridine dyes can strongly bind to DNA, intercalating between the base pairs (see, for example, Refs. 52–55). On the other hand, the triphenyl methane dyes, also positively charged, cannot totally intercalate because of their nonplanar structure. These dyes rather bind to the phosphate groups outside of the DNA molecule. An outside binding is energetically much weaker than the intercalation,[53,54] therefore we expected that the amino acridine dye would mainly bind to DNA, and the triphenyl methane dye would mainly bind to the scattering particles.

The high-polymer calf thymus DNA (Sigma Chemical Co., St. Louis, MO) was used as received. All solutions containing DNA, and the corresponding control solutions without fluorophores, were prepared in a 0.15 M phosphate buffer. The concentration of PF in our solutions was 2.2×10^{-6} M, and the concentration of DNA phosphates was 2.4×10^{-4} M. The *dye/base-pair* ratio was about 1:50, so the average distance between PF molecules was greater than 10 nm, and the resonant energy transfer between them was negligible. The transmission of the long-pass filter produced a redshift in the emission spectra of the PF-DNA complex from 503 to 515 nm. This does not affect the internal-absorption-effect correction test because all compared emission spectra were measured with the same filter.

The solutions with the Kiton Red (KR) dye, and the corresponding control solutions, were prepared in de-ionized water. Concentration of KR dye was 0.5×10^{-6} M, and the contribution of this dye into the linear absorption coefficient was $\mu_{fx}(565) = 0.013\ \mathrm{mm}^{-1}$ at the maximum of its absorption band. The concentrations of BF dye are indicated on the corresponding graphs.

The Intralipid (Kabi Pharmacia Inc., Clayton, NC) was obtained as a 10% aqueous solution and was diluted to the necessary concentrations determined from the formulas reported by van Staveren et al.[56] To obtain the solution with the MFP of 0.13 mm at 550 nm, the stock solution was diluted ×2. To obtain the solution with the MFP of 0.25 mm, the ×3.75 dilution was used, and the ×15 dilution resulted in the MFP of 1 mm at 550 nm. No traces of precipitation were noticed in the Intralipid solutions with dyes. No deterioration of the solutions within the time of the experiments was observed. The normalized absorption spectra of the PF-DNA complex in a pure buffer, and the BF and KR dyes in aqueous solutions are shown in Figure 4.

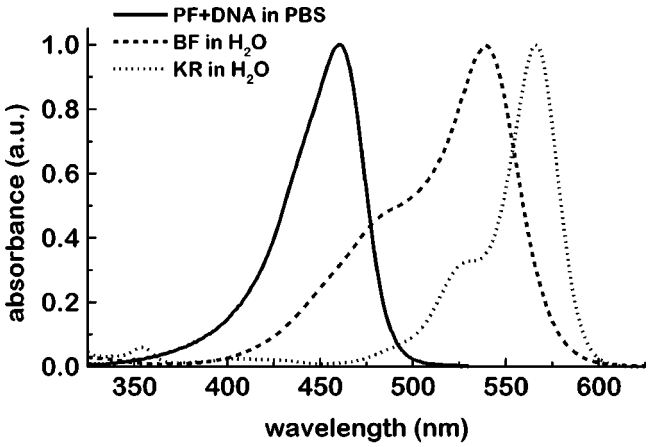

Fig. 4 Absorption spectra of the dyes: Proflavine in the complex with DNA, Basic Fuchsine, and Kiton Red. The spectra are normalized to the unit maximum absorption.

4.3 RETRIEVING THE LIGHT-ABSORPTION PROPERTIES FROM THE DIFFUSE REFLECTANCE SPECTRA

Information about the light absorption can be obtained from the diffuse reflectance spectrum $R(\lambda)$, using Eq. (8) which transforms $R(\lambda)$ into the darkness spectrum $\delta(\lambda)$, which is the ratio [Eq. (7)] of the absorption coefficient and the reduced scattering coefficient.

Figure 5 shows an example of the experimental reflectance spectrum (curve R) from the strongly scattering 2.7% Intralipid aqueous solution with the BF dye. The reflection standard was used as a reference sample. This resulting darkness spectrum is shown as the curve δ. This spectrum almost coincides in the shape with the spectrum transformed using the well-known Kubelka–Munk formula,[57,58] however our formula yields values of μ_a/μ_s' that

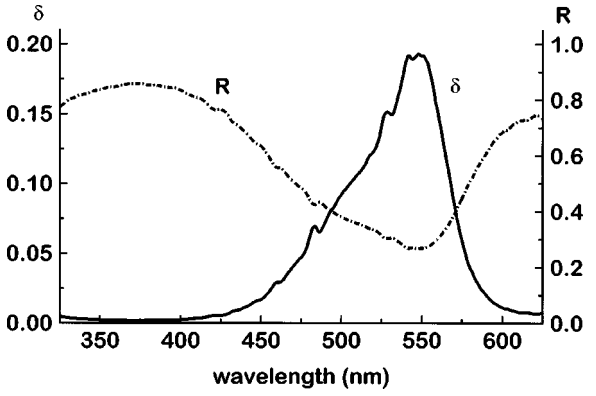

Fig. 5 Experimental diffuse reflectance spectrum (curve R) from the 2.7% Intralipid solution with 0.24 mM BF dye, and the darkness spectrum (curve δ) obtained from R using Eq. (8).

are about five times lower than the corresponding values obtained from the Kubelka–Munk formula.

We compared the darkness values δ obtained from Eq. (8) with the independently calculated ratios μ_a / μ_s'. The darkness value at the wavelength 540 nm, near the maximum of the BF absorption, $\delta(540) = 0.19$ was obtained using Eq. (8) from the diffuse reflectance spectrum as shown in Figure 5. The value of the absorption coefficient $\mu_a(540) = 0.64\ \mathrm{mm}^{-1}$ was obtained from the directly measured absorption spectrum of the solution with the same concentration of BF dye, but without scatterer. The reduced scattering coefficient $\mu_s'(540) = 4.0\ \mathrm{mm}^{-1}$ was determined from the formulas reported by van Staveren et al.[56] The calculated ratio is $\mu_a(540) / \mu_s'(540) = 0.16$, which differs from the spectral value of the darkness $\delta(540)$ within 20%. This shows that our Eq. (8) for the ratio of the absorption and the reduced scattering coefficients is in a good quantitative agreement with the experiment.

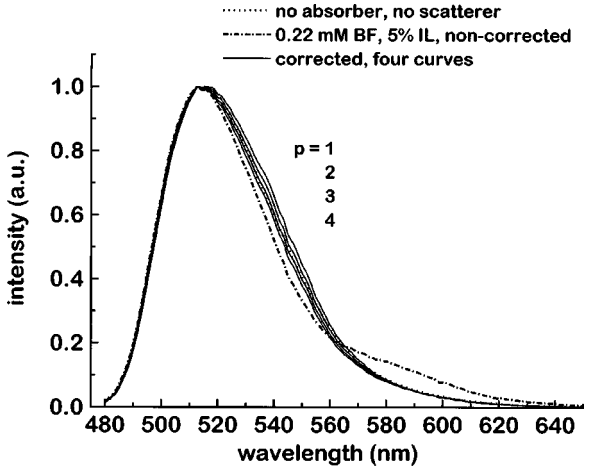

Fig. 6 Effect of the power p on the internal absorption correction in the fluorescence emission spectrum from PF-DNA complex in the 5% Intralipid solution. Excitation wavelength: $\lambda_x = 440$ nm. The spectra are normalized in the maxima.

4.4 CORRECTION OF FLUORESCENCE EMISSION SPECTRA

Figures 6–9 show the experimental testing of our procedure for the internal absorption correction in the fluorescence emission spectra. In all these figures, the dotted curves show the fluorescence emission spectra from the PF-DNA fluorescing complex in the 0.15 M phosphate buffer solution with the same concentration as in all other measurements. The emission spectra from similar samples containing the Intralipid scatterer have practically the same profile, and are not shown. The profiles of these spectra are close to the true emission spectrum. In Figures 6–8, the dashed and dot-dashed curves represent the fluorescence emission spectra of the PF-DNA complex in the 5% Intralipid solution, distorted by the inner-filter effect caused by the nonfluorescent BF dye added in different concentrations to the sample. The correction factors were calculated [Eqs. (8) and (19)] from the corresponding diffuse reflectance spectra, and every experimental fluorescence spectrum was divided [Eq. (17)] by its correction factor. All the resulting corrected spectra were normalized to the unit maximum intensity and plotted as the solid curves.

Figure 6 presents the emission spectra corrected with different values of the parameter p in Eq. (19). The effect of this parameter is noticeable, but not very strong. The best restoration of the true profile was obtained with $p = 3$. We used this value for the correction of all other emission spectra presented in Figures 7–9.

Figure 7 shows that the distortion of the fluorescence spectrum due to the inner-filter effect is more pronounced when the medium absorption is stronger. In the spectral region of the distortion, the linear absorption coefficient was $\mu_a(550) = 0.21\ \mathrm{mm}^{-1}$ for the dashed curve, and $\mu_a(550) = 0.48\ \mathrm{mm}^{-1}$ for the dot-dashed curve. The corrected spectra (solid curves) practically coincide and are very close to the true spectrum.

A similar comparison is done for the three different excitation wavelengths: 460 nm, at the maximum of the absorption band of PF-DNA (see Figure 4); 440 and 420 nm, at levels of about 2/3 and 1/3 of the maximum absorption, respectively. The corresponding values of the fluorophore contributions into the absorption coefficient are $\mu_{\mathrm{fx}}(460) = 0.0185\ \mathrm{mm}^{-1}$, $\mu_{\mathrm{fx}}(440) = 0.0126\ \mathrm{mm}^{-1}$, and $\mu_{\mathrm{fx}}(420) = 0.0062\ \mathrm{mm}^{-1}$. The apparent fluorescence emission spectra (dashed curves in Figure 8) show a stronger distortion by the inner-filter effect for the excitation wavelengths where absorption is weaker. The corrected spectra, as in the previous case, are

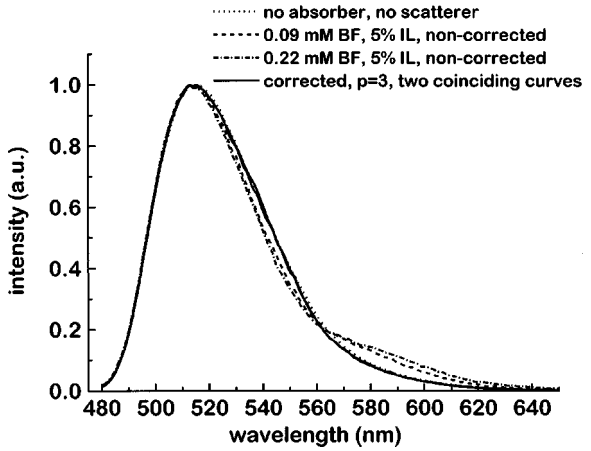

Fig. 7 Correction of the internal absorption effect in the fluorescence emission spectra from PF-DNA complex in the 5% Intralipid solution with two different concentrations of the absorber dye (BF). The correction was done using the power $p = 3$. Excitation wavelength: $\lambda_x = 440$ nm. The spectra are normalized in the maxima.

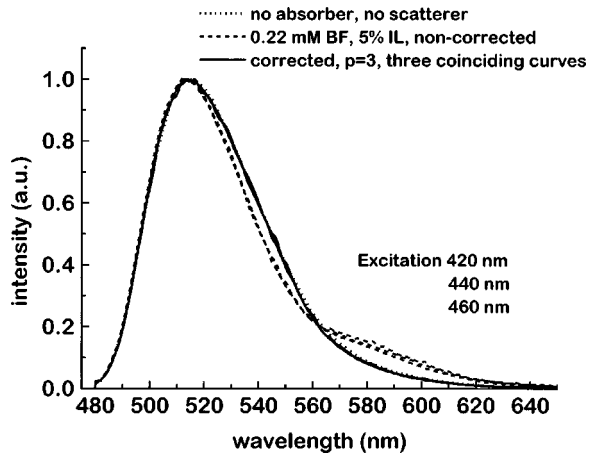

Fig. 8 Correction of the fluorescence emission spectra measured with different excitation wavelengths: 460 nm (in the maximum of the absorption), 440 nm (at about 2/3 of the maximum absorption), and 420 nm (at about 1/3 of the maximum absorption). The PF-DNA complex in the 5% Intralipid solution with the absorber dye (BF). The correction was done using the power $p=3$. The spectra are normalized in the maxima.

very close to the true spectrum and practically coincide.

Figure 9 shows the correction of the fluorescence emission spectra from PF-DNA complex in the Intralipid solutions corresponding to the photon MFP values $l \approx 0.13$ mm, $l \approx 0.25$ mm, and $l \approx 1$ mm. For the shortest MFP, which is well within the limits of the validity of our approach, the corrected spectrum is very close to the true spectrum (the upper graph in Figure 9, and Figures 6–8). The inner-filter distortion is strongest for the longest MFP of photons (1 mm), as could be expected for higher values of darkness. Though our approach is not supposed to be valid in this case, the corrected spectrum is affordably close to the true spectrum.

Similar results were obtained for suspensions of latex beads of two different sizes. There was a close similarity of the spectra to those from the Intralipid solutions. Some difference was found in the optimal value of the power p in Eq. (19). For the spectra from the samples with the beads of 0.198 μm diameter, the best correction was obtained with $p=2$–3, as for the Intralipid solutions, while for the beads of 1.07 μm diameter this value turns out to be closer to 1, which naturally comes from the larger size of the particles.

4.5 CORRECTION OF FLUORESCENCE EXCITATION SPECTRA

On the upper graph of Figure 10 the dotted curve shows the nondistorted fluorescence excitation spectrum of KR dye in the aqueous solution without the added absorber and without the scatterer. The spectrum for the sample with the same concentration of KR in 2.7% Intralipid solution is very close in shape to the dotted curve and is not shown. After the BF dye in the concentration of 0.24 mM is

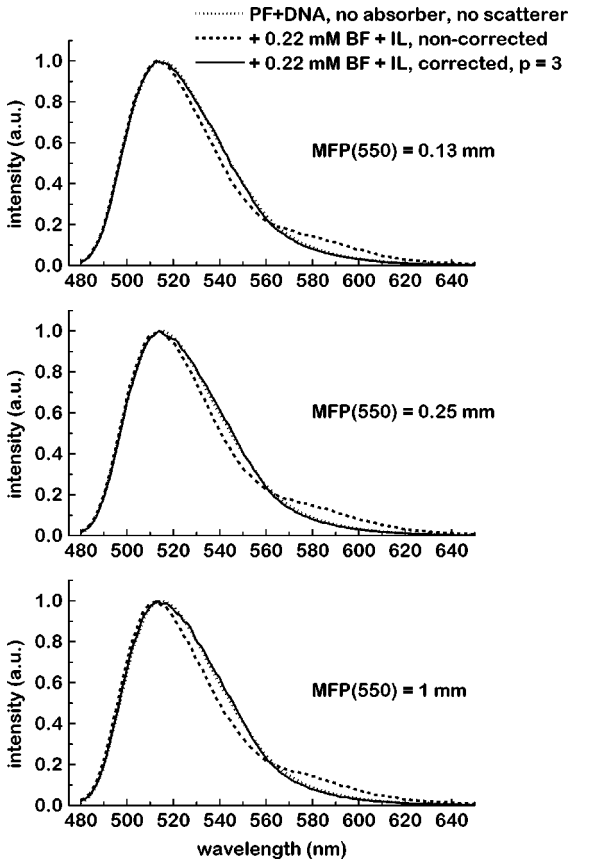

Fig. 9 Correction of the internal absorption effect in the fluorescence emission spectra from the PF-DNA complex in the Intralipid solutions with different values of the photon MFP. The correction was done using the power $p=3$. Excitation wavelength: $\lambda_x = 440$ nm. The spectra are normalized in the maxima.

added to this sample, the excitation spectrum of KR dye (dashed curve) appears distorted. The correction factors were calculated from the diffuse reflectance spectra using Eqs. (8) and (22). The experimental excitation spectra were divided by their correction factors and normalized to the unit maximum intensity. Four corrected spectra, for different values of the power p in Eq. (22), are shown as the solid curves. The curves for $p=2$ and $p=3$ are the closest in shape to the nondistorted spectrum. The lower graph in Figure 10 compares the correction results for two different concentrations of the absorber. The linear absorption coefficients in the spectral region of the distortion were $\mu_a(550) = 0.52\ \mathrm{mm}^{-1}$ for the dashed curve, and $\mu_a(550) = 1.31\ \mathrm{mm}^{-1}$ for the dot-dashed curve. The curves do not differ significantly, which is in agreement with the prediction of our model: a distortion of the excitation spectrum arises at low values of darkness of the medium, and this distortion does not increase much with a further increase of the darkness. The corrected spectra (solid curves) for both concentrations almost coincide and are close in shape to the nondistorted excitation spectrum (the dotted curve). A difference (short-wavelength shift of the

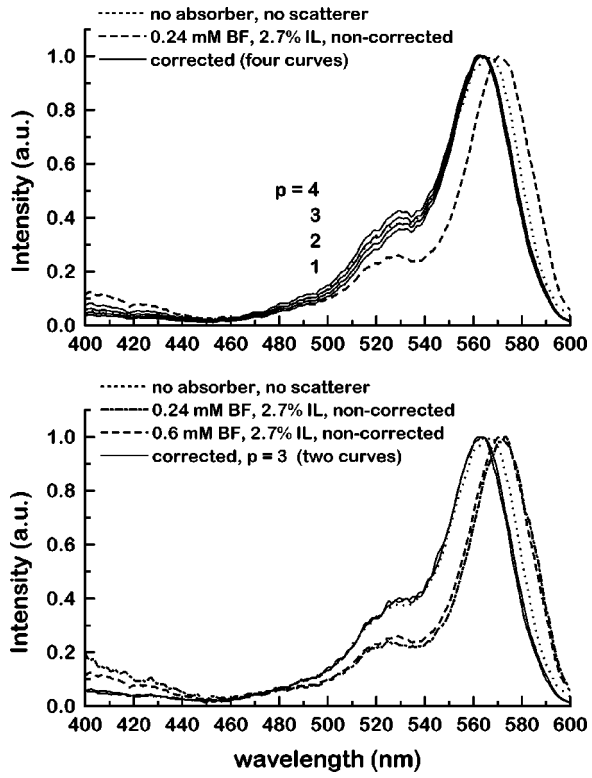

Fig. 10 Correction of the fluorescence excitation spectra of the Kiton Red dye in the 2.7% Intralipid solution. The absorber dye was BF; emission wavelength: $\lambda_m = 620$ nm. The upper graph shows the results of the correction using different values of the power p. The lower graph shows the correction, with the power $p = 3$, for two different concentrations of the absorber. The spectra are normalized in the maxima.

maximum) between the corrected spectra and the spectrum from the sample without the absorber and without the scatterer can be attributed to the effect of reemission of photons absorbed by KR dye, which is not accounted for in our model.

5 DISCUSSION

The experimental results presented in Figures 6–8 and the upper graphs of Figure 9 show that our correction method eliminates the spectral distortions produced by the inner-filter effect in fluorescence emission spectra from highly scattering media when the MFP is within the range of validity of our model. The reflectances in our experiments were in the range $R = 0.85$–0.1, which corresponds to the values of darkness $\delta = 0.004$–0.9. These values, and three values of the photon MFPs (transport lengths) of 0.13, 0.25, and 1 mm, are in the ranges of parameters usually found in biological tissues, such as breast and brain. The highest values of darkness and photon MFP exceed the margins of the validity of our mathematical approach in our experimental conditions. Nevertheless, even in these conditions our correction method satisfactorily restored the profile of the true fluorescence emission spectrum. This means that our model can work in a wider range of parameters than it is formally supposed to do. It would be interesting to test our correction procedure in a broader range than we did, but the stray light of the spectrometer and coagulation of the scattering particles preclude this now.

Our experiments on the correction of excitation spectra were done in nonideal conditions due to the difficulties imposed by the stray light of the spectrometer. The data presented in Figure 10 show that our method satisfactorily restores the true excitation spectrum. However, further testing of the excitation correction method is needed.

We do not consider the reported experimental testing as a full validation of the method. This validation requires more comprehensive testing. The margins of the applicability of the method have not been reached yet and must be established later. We think that the method can be cautiously applied to some biological samples, in which the inhomogeneities have the dimensions much greater than the photon MFP. Our method is not supposed to be applicable to thin-layered or strongly nonuniform media.

Our method for internal absorption effect correction can be easily implemented technically. The correction algorithms for both emission and excitation spectra do not require any lengthy and time-consuming computer processing and can be performed on practically any personal computer. Full mathematical processing of 100 spectra on a Pentium 100 MHz computer using a self-made extension to the LabCalc software (Galactic Industries Corp.) takes a few seconds. Running one additional, synchroscan, spectrum requires only a duplication of the scanning time that usually varies from a few seconds to several minutes.

6 CONCLUSION

A direct method was developed and experimentally tested, which can correct the internal light-absorption effect in fluorescence emission and excitation spectra from moderately absorbing and highly scattering media. The true fluorescence emission or excitation spectrum is obtained from the measured fluorescence spectrum by dividing it by a wavelength-dependent correction factor that is directly calculated from the diffuse reflectance spectrum measured from the same position on the sample. The method is simple for technical implementation and allows rapid spectral correction.

Acknowledgments

We express our gratitude to Dr. N. Ockman, Dr. A. Polishchuk, Dr. S. Demos, Dr. F. Liu, Dr. L. Wang, Dr. A. Gorokhovsky, and A. Turukhin for helpful discussions. We thank G. Minko for his comments about the text. We also thank the reviewers whose comments helped to considerably improve the article. This work was supported in part by the Me-

discience Technology Corp. and the New York State Science and Technology Foundation.

REFERENCES

1. R. R. Alfano, D. B. Tata, J. Cordero, P. Tomashefsky, F. W. Longo, and M. A. Alfano, ''Laser induced fluorescence spectroscopy from native cancerous and normal tissue,'' *IEEE J. Quantum Electron.* **QE-20**(12), 1507–1511 (1984).
2. J. R. Lakowicz, *Principles of Fluorescence Spectroscopy*, Plenum Press, New York (1983).
3. C. H. Liu, G. C. Tang, A. Pradhan, W. L. Sha, and R. R. Alfano, ''Effects of self-absorption by hemoglobins on the fluorescence spectra from normal and cancerous tissues,'' *Lasers Life Sci.* **3**, 167–176 (1990).
4. S. A. Ahmed, Z. W. Zang, K. M. Yoo, and R. R. Alfano, ''Effect of multiple light scattering and self-absorption on the fluorescence and excitation spectra of dyes in random media,'' *Appl. Opt.* **33**, 2746–2750 (1994).
5. A. Ishimaru, *Wave Propagation and Scattering in Random Media*, Vol. I, Academic Press, New York (1978).
6. D. M. Benson and J. A. Knopp, ''Effect of tissue absorption and microscope optical parameters on the depth of penetration for fluorescence and reflectance measurements of tissue samples,'' *Photochem. Photobiol.* **39**, 495–502 (1984).
7. A. E. Profio and D. R. Doiron, ''Transport of light in photodynamic therapy,'' *Photochem. Photobiol.* **46**, 591–599 (1987).
8. R. J. Crilly, W.-F. Cheong, B. C. Wilson, and J. R. Spears, ''Application of the adjoined method to Monte Carlo studies of fluorescent localization in turbid media,'' *Proc. SPIE* **2135**, 82–93 (1994).
9. R. Cubeddu, G. Canti, M. Musolino, A. Pifferi, P. Taroni, and G. Valentini, ''Absorption spectrum of hematoporphyrin derivative in vivo in a murine tumor model,'' *Photochem. Photobiol.* **60**, 582–585 (1994).
10. D. Oelkrug, M. Brun, and U. Mammel, ''Spatial fluorescence profiles in multiple light scattering systems,'' *J. Lumin.* **60–61**, 422–425 (1994).
11. I. V. Meglinsky, Y. P. Sinichkin, S. R. Utz, and H. A. Pilipenko, ''Simulation of fluorescence measurements in human skin,'' *Proc. SPIE* **2389**, 621–631 (1995).
12. T. H. Morton, ''Optical studies III—Fluorescent brightening agents on textiles: Elementary optical theory and its practical implications,'' *J. Soc. Dyers Colourists* **79**, 238–242 (1963).
13. E. Allen, ''Fluorescent white dyes: Calculation of fluorescence from reflectivity values,'' *J. Opt. Soc. Am.* **54**, 506–515 (1964).
14. R. Richards-Kortum, R. P. Rava, M. Fitzmaurice, L. L. Tong, N. B. Ratliff, J. R. Kramer, and M. S. Feld, ''A one-layer model of laser-induced fluorescence for diagnosis of disease in human tissue: Applications to atherosclerosis,'' *IEEE Trans. Biomed. Eng.* **36**, 1222–1232 (1989).
15. M. Sinaasappel and H. J. C. M. Sterenborg, ''Quantification of the hematoporphyrin derivative by fluorescence measurement using dual-wavelength excitation and dual-wavelength detection,'' *Appl. Opt.* **32**, 541–548 (1993).
16. S. Warren, K. Pope, Y. Yazdi, A. J. Welch, A. L. Johnston, M. J. Davis, and R. Richards-Kortum, ''Combined ultrasound and fluorescence spectroscopy for physico-chemical imaging of atherosclerosis,'' *IEEE Trans. Biomed. Eng.* **42**, 121–132 (1995).
17. M. Keijzer, R. Richards-Kortum, S. L. Jacques, and M. S. Feld, ''Fluorescence spectroscopy of turbid media: Autofluorescence of the human aorta,'' *Appl. Opt.* **28**, 4286–4292 (1989).
18. A. J. Durkin, S. Jaikumar, N. Ramanujam, and R. Richards-Kortum, ''Relation between fluorescence spectra of dilute and turbid samples,'' *Appl. Opt.* **33**, 414–423 (1994).
19. J. Wu, F. Partovi, M. S. Feld, and R. P. Rava, ''Diffuse reflectance from turbid media: An analytical model of photon migration,'' *Appl. Opt.* **32**, 1115–1121 (1993).
20. J. Wu, M. S. Feld, and R. P. Rava, ''Analytical model for extracting intrinsic fluorescence in turbid media,'' *Appl. Opt.* **32**, 3585–3595 (1993).
21. M. S. Patterson and B. W. Pogue, ''Mathematical model for time-resolved and frequency-domain fluorescence spectroscopy in biological tissues,'' *Appl. Opt.* **33**, 1963–1974 (1994).
22. C. L. Burch, J. R. Lakowicz, and E. M. Sevick-Muraca, ''Biochemical sensing in tissues: Determination of fluorescence lifetimes in multiply scattering media using frequency-domain fluorescence spectroscopy,'' *Proc. SPIE* **2135**, 286–299 (1994).
23. E. M. Sevick-Muraca and C. L. Burch, ''Origin of phosphorescence signals reemitted from tissues,'' *Opt. Lett.* **19**, 1928–1930 (1994).
24. C. L. Hutchinson, J. R. Lakowicz, and E. M. Sevick-Muraca, ''Fluorescence lifetime-based sensing in tissues: A computational study,'' *Biophys. J.* **68**, 1574–1582 (1995).
25. E. M. Sevick-Muraca and C. L. Hutchinson, ''Probability description of fluorescent and phosphorescent signal generation in tissues and other random media,'' *Proc. SPIE* **2387**, 274–283 (1995).
26. C. L. Hutchinson, T. L. Troy, and E. M. Sevick-Muraca, ''Fluorescence lifetime spectroscopy and imaging in random media,'' *Proc. SPIE* **2389**, 274–283 (1995).
27. D. Y. Paithankar, A. Chen, and E. M. Sevick-Muraca, ''Fluorescent yield and lifetime imaging in tissues and other scattering media,'' *Proc. SPIE* **2679**, 71–78 (1996).
28. J. S. Maier, A. E. Cerussi, S. Fantini, M. A. Franceschini, and E. Gratton, ''Quantitative fluorescence in tissue-like media,'' *Biomedical Optical Spectroscopy and Diagnostics*, D. Benaron and E. Sevick-Muraca, Eds., pp. 206–209, 1996 OSA Technical Digest, Optical Society of America, Washington, DC (1996).
29. A. Cerussi, J. S. Maier, S. Fantini, M. A. Franceschini, W. W. Mantulin, and E. Gratton, ''Experimental verification of a theory for the time-resolved fluorescence spectroscopy of thick tissues,'' *Appl. Opt.* **36**, 116–124 (1997).
30. A. Cerussi, S. Fantini, M. A. Franceschini and E. Gratton, ''Frequency-domain lifetime spectroscopy in the multiple scattering regime,'' (Abstract) *Biophys. J.* **72**, A211 (1996).
31. T. French, A. Cerussi, S. Fantini, M. A. Franceschini, and E. Gratton, ''Measurement of absolute fluorescence quantum yield in turbid media,'' (Abstract) *Biophys. J.* **72**, A211 (1996).
32. X. D. Li, M. A. O'Leary, D. A. Boas, B. Chance, and A. G. Yodh, ''Fluorescent diffuse photon density waves in homogeneous and heterogeneous turbid media: Analytic solutions and applications,'' *Appl. Opt.* **35**, 3746–3758 (1996).
33. A. H. Gandjbakhche, R. F. Bonner, I. Gannot, J. Knutson, R. Navai, R. Nossal, and G. H. Weiss, ''Fluorescent photon migration theory for turbid biological media,'' *Proc. SPIE* **2679**, 8–15 (1996).
34. L. Reynolds, C. Johnson, and A. Ishimaru, ''Diffuse reflectance from a finite blood medium: Application to the modeling of fiber optic catheters,'' *Appl. Opt.* **15**, 2059–2067 (1976).
35. R. A. J. Groenhuis, H. A. Ferwerda, and J. J. Ten Bosh, ''Scattering and absorption of turbid materials determined from reflection measurements, 1: Theory,'' *Appl. Opt.* **22**, 2456–2462 (1983).
36. B. C. Wilson and M. S. Patterson, ''The physics of photodynamic therapy,'' *Phys. Med. Biol.* **31**, 327–360 (1986).
37. M. Lax, V. Nayaramamurti, and R. C. Fulton, ''Classical diffusive photon transport in a slab,'' in *Proceedings of the Symposium on Laser Optics of Condensed Matter*, J. L. Birman, H. Z. Cummings, and A. A. Kaplyanskii, Eds., pp. 229–235, Plenum, New York (1987).
38. M. S. Patterson, B. Chance, and B. C. Wilson, ''Time resolved reflectance and transmittance for the non-invasive measurements of tissue optical properties,'' *Appl. Opt.* **28**, 2231–2236 (1989).
39. G. Yoon, S. P. Prahl, and A. J. Welch, ''Accuracies of the diffusion approximation and its similarity relations for laser irradiated biological media,'' *Appl. Opt.* **28**, 2250–2255 (1989).
40. S. T. Flock, M. S. Patterson, B. C. Wilson, and D. R. Wyman, ''Monte Carlo modeling of light propagation in highly scattering tissues-I: Model predictions and comparison with diffusion theory,'' *IEEE Trans. Biomed. Eng.* **36**, 1162–1173 (1989).
41. J. L. Karagiannes, Z. Zhang, B. Grossweiner, and L. I. Grossweiner, ''Applications of the 1-D diffusion approximation to

the optics of tissues and tissue phantoms,'' *Appl. Opt.* **28**, 2311–2317 (1989).
42. K. M. Yoo, Feng Liu, and R. R. Alfano, ''When does the diffusion approximation fail to describe photon transport in random media?'' *Phys. Rev. Lett.* **64**, 2647–2650 (1990). Erratum **65**, 2210–2211 (1990).
43. S. J. Madsen, B. C. Wilson, M. S. Patterson, Y. D. Park, S. L. Jacques, and Y. Hefetz, ''Experimental tests of a simple diffusion model for the estimation of scattering and absorption coefficients of turbid media from time-resolved diffuse reflectance measurements,'' *Appl. Opt.* **31**, 3509–3517 (1992).
44. B. C. Wilson, E. M. Sevick, M. S. Patterson, and B. Chance, ''Time-dependent optical spectroscopy and imaging for biomedical applications,'' *Proc. IEEE* **80**, 918–930 (1992).
45. F. Liu, K. M. Yoo, and R. R. Alfano, ''Should the photon flux or the photon density be used to describe the temporal profiles of scattered ultrashort laser pulses in random media?'' *Opt. Lett.* **18**, 432–434 (1993).
46. J. B. Fishkin and E. Gratton, ''Propagation of photon-density waves in strongly scattering media containing an absorbing semi-infinite plane bounded by a straight edge,'' *J. Opt. Soc. Am. A* **10**, 127–140 (1993).
47. E. M. Sevick-Muraca, ''Computations of time-dependent photon migration for biomedical optical imaging,'' *Methods in Enzymology* **240**, 748–781 (1994).
48. W.-F. Cheong, S. A. Prahl, and A. J. Welch, ''A review of the optical properties of biological tissues,'' *IEEE J. Quantum Electron.* **26**, 2166–2185 (1990).
49. V. G. Peters, D. R. Wyman, M. S. Patterson, and G. L. Frank, ''Optical properties of normal and diseased human breast tissues in the visible and near infrared,'' *Phys. Med. Biol.* **35**, 1317–1334 (1990).
50. J. B. Birks, *Photophysics of aromatic molecules*, Wiley-Interscience, London (1970).
51. M. Motamedi, S. Rastegar, G. LeCarpentier, and A. J. Welch, ''Light and temperature distribution in laser irradiated tissue: The influence of anisotropic scattering and refractive index,'' *Appl. Opt.* **28**, 2230–2237 (1989).
52. L. S. Lerman, ''Structural considerations in the interaction of DNA and acridines,'' *J. Mol. Biol.* **3**, 18–30 (1961).
53. H. J. Li and D. M. Crothers, ''Relaxation studies of the Proflavine-DNA complex: The kinetics of the intercalation reaction,'' *J. Mol. Biol.* **39**, 461–477 (1969).
54. R. W. Armstrong, T. Kuruscev, and U. P. Strauss, ''The interaction between acridine dyes and deoxyribonucleic acid,'' *J. Amer. Chem. Soc.* **92**, 3174–181 (1970).
55. N. N. Zhadin and V. L. Rapoport, ''Spectroscopic features of different types of Acriflavine-DNA binding in ultraviolet and visible region,'' *Molec. Biol.* **9**, 233–239 (1975).
56. H. J. van Staveren, C. J. Moes, J. van Marle, S. A. Prahl, and M. J. C. van Gemert, ''Light scattering in Intralipid-10% in the wavelength range 400–1100 nm,'' *Appl. Opt.* **30**, 4507–514 (1991).
57. P. Kubelka and F. Munk, ''Ein beitrag zur optik der farbanstriche,'' *Z. Tech. Phys.* **12**, 593 (1931).
58. P. Kubelka, ''New contributions to the optics of intensely light-scattering materials,'' *J. Opt. Soc. Am.* **38**, 448–457 (1948). Erratum **38**, 1067 (1948).